Design principles for Bernal spirals and helices with tunable pitch

Szilard N. Fejer[a,b],[*] Dwaipayan Chakrabarti[c],[†]

Halim Kusumaatmaja[d],[‡] and David J. Wales[e][§]

[a] *Department of Chemical Informatics,*

University of Szeged, Faculty of Education,

Boldogasszony sgt. 6, H-6725 Szeged, Hungary

[b] *Pro-Vitam Ltd., str. Muncitorilor nr. 16, 520032 Sfantu Gheorghe, Romania*

[c] *School of Chemistry, University of Birmingham,*

Edgbaston, Birmingham B15 2TT, United Kingdom

[d] *Department of Physics, Durham University,*

South Road, Durham DH1 3LE, United Kingdom

[e] *University Chemical Laboratories, Lensfield Road,*

Cambridge CB2 1EW, United Kingdom

Abstract

Using the framework of potential energy landscape theory, we describe two *in silico* designs for self-assembling helical colloidal superstructures based upon dipolar dumbbells and Janus-type building blocks, respectively. Helical superstructures with controllable pitch length are obtained using external magnetic field driven assembly of asymmetric dumbbells involving screened electrostatic as well as magnetic dipolar interactions. The pitch of the helix is tuned by modulating the Debye screening length over an experimentally accessible range. The second design is based on building blocks composed of rigidly linked spheres with short-range anisotropic interactions, which are predicted to self-assemble into Bernal spirals. These spirals are quite flexible, and longer helices undergo rearrangements *via* cooperative, hinge-like moves, in good agreement with experiment.

keywords: self-assembly, chirality, Bernal spirals, Janus particles, mesoscopic modelling

[*]Electronic address: `szilard.fejer@cantab.net`

[†]Electronic address: `d.chakrabarti@bham.ac.uk`

[‡]Electronic address: `halim.kusumaatmaja@durham.ac.uk`

[§]Electronic address: `dw34@cam.ac.uk`

I. INTRODUCTION

The ubiquitous presence of helical architectures in nature, as well as their diverse potential applications in materials science, for optoelectronics [1], sensors [2], responsive materials [3], and asymmetric catalysis [4], has motivated interest in design and synthesis. Molecular self-assembly, in particular, is a promising route to helicity [2, 5]. Self- or directed-assembly of nanoparticles and colloidal building blocks has enormous potential as a means of fabrication because of the scope for tuning the interactions [6, 7]. A delicate balance between a variety of weak forces often governs the assembled structure [8]. A thorough understanding of these forces holds the key to rational design.

The present contribution reports on two complementary routes to helical nanostructures, starting from anisotropic building blocks. The first strategy employs directed assembly of achiral colloidal building blocks [9, 10], where an interplay between two length scales for the anisotropic interactions determines the emergent chirality of the nanostructure. Such competing length scales are present in DNA [11], one characterising the distance between consecutive nucleotides in the sugar-phosphate backbone, and the other governing the stacking of the base pairs. Here the competing length scales arise due to electrostatic and magnetic dipolar interactions. While much progress has been made in obtaining emergent chirality from achiral building blocks, biasing the superstructure to a particular handedness [12], or controlling the pitch [13], has proved more difficult. We address the latter challenge using theory and simulation, and demonstrate that significant control (around 30%) over the pitch length can be achieved by modulating the Debye screening length of the electrostatic interactions over an experimentally accessible range. The resulting tunable pitch length for helical superstructures holds significant promise for the design of a novel class of responsive materials.

The second design principle considered here involves clusters of Janus particles. Several models have been used recently to study the dynamics and aggregation properties of systems composed of Janus-type building blocks [14–17], and the resulting phase diagrams exhibit a wide variety of potential target morphologies for self-assembly, depending on the anisotropic properties (shape and interactions). Interestingly, none of the models employed so far was able to reproduce assembly into Bernal spirals (BC spirals or tetrahelices) from anisotropic building blocks, although such systems have been designed and observed experimentally [18].

Here we report the design of a Janus building block that prefers assembly into Bernal spirals, suitably guided by experimentally relevant, anisotropic interaction potentials [14, 18].

Assembly into one-dimensional polytetrahedral clusters, locally organized as Bernal spirals, has been achieved previously for isotropic particles as well [19], and reproduced computationally, by tuning the balance between a long-range screened isotropic repulsion and a short-range attraction term in the potential [20, 21].

II. METHODS

We have used basin-hopping global optimisation [22–24] as implemented in the `GMIN` program [25] to predict global minima. Basin-hopping global optimisation involves perturbations of geometry followed by energy minimisation. The perturbations are designed to avoid any overlapping particles. For the dipolar dumbbells, we run 50000 basin-hopping steps for each set of parameters presented in this paper. Global minima for Janus clusters have been identified by running 10000 basin-hopping steps for at least 10 random starting structures.

The energy landscapes for 20 and 24 Janus particles described in §IV were explored using double-ended pathway searches between local minima with the discrete path sampling [26–28] approach, as implemented in our `OPTIM` [29] and `PATHSAMPLE` [30] programs. We have employed the doubly-nudged [31] elastic band [32–34] (DNEB) method [35] to locate transition state candidates. The method has been adapted to avoid overlapping geometries for Janus building blocks, by diagnosing overlap between the ellipsoids in each interpolated structure and moving the overlapping ellipsoids by small random amounts until there is no overlap in the cluster. Transition states were refined using gradient-only hybrid eigenvector-following [36] from TS candidates identified with the DNEB algorithm. The most likely rearrangement mechanisms (pathways with the largest contribution to the steady-state rate constant ignoring recrossings [28]) were obtained using Dijkstra analysis [37] of the resulting kinetic transition network.

To visualise the corresponding multidimensional potential energy surfaces we construct disconnectivity graphs [38, 39] from the databases of minima and transition states explored during discrete path sampling. Further details of all the geometry optimisation and visualisation techniques exploited in this potential energy landscapes framework can be found in

previous reports and reviews [28, 40–42].

III. CONTROLLABLE HELIX PITCH

A. A Decorated Rigid Body Model

The colloidal building blocks considered here are charged dipolar asymmetric dumbbells, which involve screened electrostatic as well as dipolar interactions. We modelled these particles using multiple interaction sites that decorate a rigid framework. Each dumbbell involves two lobes, each modelled by a spherically symmetric effective Yukawa pair potential [43, 44], where the inverse screening length κ controls the range as well as the softness of the screened electrostatic interactions, which can be tuned in experiment by modulating the salt concentration of the medium [44, 45]. Additionally, there is a magnetic point dipole between the lobes, directed perpendicular to the axis. Such interaction may be realized experimentally, e.g. using emulsion confinement [10], where densely packed magnetic nanoparticles form a ring around two contacting silica spheres. The total energy of a system of N such dumbbells in an external magnetic field $\boldsymbol{B}$ is given by

$$
\begin{aligned}
U = {} & \sum_{I=1}^{N-1} \sum_{J=I+1}^{N} \sum_{i \in I}^{1,2} \sum_{j \in J}^{1,2} \epsilon_{ij} \frac{\exp[-\kappa(r_{ij} - \sigma_{ij})]}{r_{ij}/\sigma_{ij}} \\
& + \sum_{I=1}^{N-1} \sum_{J=I+1}^{N} \frac{\mu_D^2}{r_{IJ}^3} \left[(\hat{\boldsymbol{\mu}}_I \cdot \hat{\boldsymbol{\mu}}_J) - 3(\hat{\boldsymbol{\mu}}_I \cdot \hat{\mathbf{r}}_{IJ})(\hat{\boldsymbol{\mu}}_J \cdot \hat{\mathbf{r}}_{IJ}) \right] - \mu_D \sum_{I=1}^{N} \hat{\boldsymbol{\mu}}_I \cdot \boldsymbol{B}.
\end{aligned}
\tag{1}
$$

Here, $\mathbf{r}_I$ is the position vector for the magnetic point dipole on dumbbell I, $\hat{\boldsymbol{\mu}}_I$ is the unit vector defining the direction of the dipole moment, whose magnitude is μ_D, $\mathbf{r}_{IJ} = \mathbf{r}_I - \mathbf{r}_J$ is the separation vector between dipoles on dumbbells I and J with magnitude r_{IJ}, $\hat{\mathbf{r}}_{IJ} = \mathbf{r}_{IJ}/r_{IJ}$, and r_{ij} is the separation between the Yukawa sites i and j. The units of energy and length are chosen as the Yukawa parameters ϵ_Y and σ_{11}, respectively. For the Yukawa interactions we set $\epsilon_{11} = \epsilon_{22} = \epsilon_{12} = 0.1\epsilon_Y$ and $\sigma_{11} = 1$. $\sigma_{22} < 1$ defines the asymmetry parameter $\alpha = \sigma_{11}/\sigma_{22}$; σ_{12} is chosen to be the arithmetic average $\sigma_{12} = (\sigma_{11} + \sigma_{22})/2$. The direction of the external field $\boldsymbol{B} = (0, 0, B)$ was held fixed along the z-axis of the space-fixed frame as its strength, B, was varied. The magnetic dipole μ_D is then in reduced units of $(4\pi\epsilon_Y\sigma_{11}^3/\mu_0)^{1/2}$ and the magnetic field strength B is in $[\epsilon_Y\mu_0/(4\pi\sigma_{11}^3)]^{1/2}$, where μ_0 is the permeability of free space. For the simulation results presented here, we have used in

4

reduced units $\mu_D = 0.1$, $B = 10.0$, $\sigma_{11} = 1.0$, $\sigma_{22} = 0.4$. κ is varied over an experimentally relevant range, as discussed in the next section.
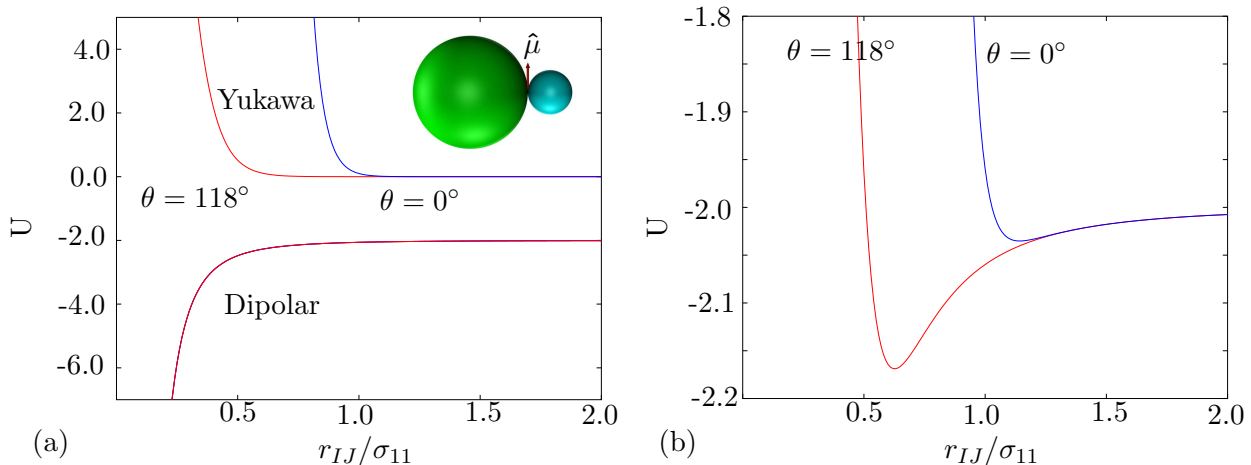

FIG. 1: The potential energy of two interacting dumbbells with $\kappa\sigma_{11} = 20$ as a function of the separation between dumbbell I and J, r_{IJ}. The other parameters are as given in the text. In panel (a), the contributions from the Yukawa and dipolar interactions are shown separately. Panel (b) shows the sum of the two contributions. In the figures, we have assumed that the direction of the dipole moment is parallel to the external field. θ is the angle between the axes of dumbbells I and J; the global minimum energy for two dumbbells is located at $\theta \sim 118°$. The inset in panel (a) shows a schematic representation of the dumbbell building block, where the point dipole perpendicular to the axis of the dumbbell is not drawn to scale.

B. Results

For small clusters, the global optimisation results reveal a helical superstructure as the ground state for an optimal asymmetry when a sufficiently strong external field is applied. The dumbbells tend to align perpendicular to the field, to facilitate alignment of the dipoles. An optimal asymmetry is critical for helix formation, because competition with a second length scale, which controls the steric interactions, is the basis of the emergent chirality [9, 10]. A single helical strand is observed without any predetermined chirality for clusters up to at least $N = 20$ for the set of parameters investigated.

Figure 1 shows that the pitch length can be controlled by modulating the range of the

5

screened electrostatic interactions, which can be tuned experimentally by changing the salt concentration of the medium [46]. It is evident that the pitch of the helix changes by nearly 30% upon varying κ over a range accessible in experiments for both $N = 9$ and $N = 20$. The slight difference between the two sizes arises due to additional (attractive) dipolar interactions when more dumbbells are present in the cluster. As κ is increased (screening length is decreased), the Yukawa potential is shorter in range and the equilibrium distance between two dumbbells decreases. The change in pitch is primarily attributed to this varying equilibrium separation, the change in twist angle being nominal. The limiting cases are insightful. For large κ, the Yukawa potential approaches a hard-sphere interaction, and for $\kappa \to 0$, it approaches the long-range Coulomb potential. Figure 2 shows that the range of the screened electrostatic interactions directly affects the helix pitch length, but helix integrity is preserved. Hence the design proposed here offers a route to helical nanostructures with controllable pitch length.

As for the parameters, a reasonable estimate in physically relevant units can be obtained by setting $\epsilon_Y = 4.1 \times 10^{-21}$ J (of the order of $k_B T$) and $\sigma_{11} = 10^{-6}$ m. In the above analysis we have neglected the screening effect on the dipolar interactions in the medium. This assumption is valid when magnetic dipoles are involved [10, 47]. In the absence of the screening effect on the magnetic interactions, the screened electrostatic and magnetic interactions can be manipulated independently.[48] The values in reduced units used here correspond to a magnetic dipole moment $\mu_D \sim 2 \times 10^{-17}$ A m^2 and a magnetic field strength $B \sim 2 \times 10^{-4}$ T, well within the experimentally accessible regime.

If we consider an aqueous medium for a monovalent electrolyte, where the ionic strength I is equal to the molar concentration, the Bjerumm length λ_B of water is 0.7 nm at 298 K, equivalent to a colloid charge of $Z \sim 130$ for the larger lobe of the dumbbell when $\kappa\sigma_{11} = 20$ using the relationship $\epsilon_{11}/(k_B T) = Z^2(\lambda_B/\sigma_{11})/(1 + \kappa\sigma/2)^2$ [49]. For the parameter range considered here, the variation of the Debye screening length κ^{-1} is between 20 nm and 80 nm. With concentrations as low as $\sim 1\,\mu M$ achievable in an experimental setup [45], this range is well within the regime accessible in experiments, since the following relationship holds: $\kappa^{-1} = 0.304\,I^{-1/2}$, where κ^{-1} is in nanometres and I is in moles per litre [50].
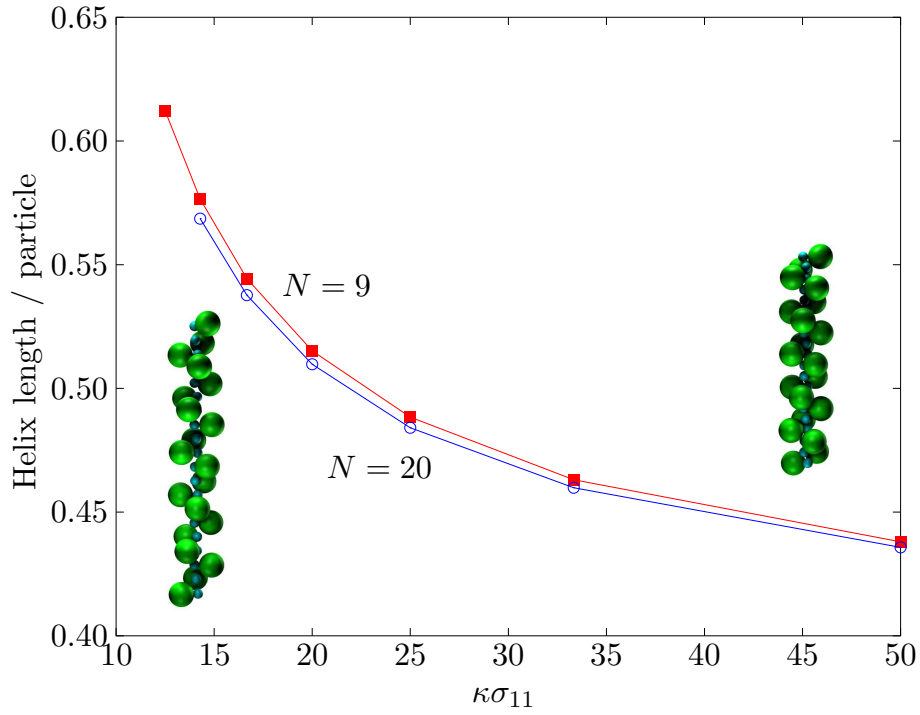
6

FIG. 2: Helix length per particle as a function of the inverse screening length for the predicted ground state structures. Results are shown for $N = 9$ and $N = 20$. Insets: the $(N = 20)$ helix configurations for (left) $\kappa\sigma_{11} = 14.3$ and (right) $\kappa\sigma_{11} = 50.0$. The dipoles are not shown for clarity of presentation.

IV.   CLUSTERS OF JANUS PARTICLES

A.   Computational Model

We have previously shown that very different interparticle potentials can produce rather similar preferred arrangements during aggregation [51], as long as the overall pair potentials are sufficiently alike. Current designs of spherical mesoscopic Janus building blocks generally involve a charged hydrophilic hemisphere combined with a hydrophobic hemisphere in an aqueous environment. Changing the ionic strength of the solution effectively changes the screening of the electrostatic repulsion, and worm-like structures arise when the charges are well screened, corresponding to short-ranged repulsive terms. Potentials that have been used for Janus particle modelling therefore usually include three types of interaction: hard sphere repulsion to prevent overlap, hydrophobic interactions, and screened Coulombic repulsion [14]. Most potentials employed to date are discontinuous, containing quasi-square

well functions and hard sphere interactions, which are not suitable for energy landscape studies based on geometry optimisation. Recently, a potential has been developed for soft Janus particles [15], but it involves considerably longer-range interactions than what we consider in the present study.

Our design for a Janus building block tries to capture the net behaviour of particles with strongly anisotropic short-range interactions in solution, aggregating around the hydrophobic hemisphere. We use continuous and differentiable functional forms, and aim to keep the potential as simple as possible, to extract the minimal conditions on the interparticle forces that correspond to particular target morphologies. The Paramonov-Yaliraki (PY) potential [52] has proved its versatility for modelling a large number of anisotropic interactions [9, 51, 53], and here we have used this representation to create Janus-type particles by modifying just two interaction parameters in the pairwise energy. Each Janus building block is composed of two rigidly linked spheres (A and B) represented by PY ellipsoids [52, 54] having the same orientation and shifted along the z axis by 0.1 distance units from the origin, in opposite directions. The building blocks interact within a rigid-body framework using the angle-axis description for the orientational degrees of freedom [55, 56]. To allow for shorter-range interactions than the usual Lennard-Jones form, we have increased the diameter of the spheres threefold, while keeping the range parameter σ_0 fixed at unity. One sphere (ellipsoid A) is purely repulsive, while the other has a higher interaction strength along the z direction (attractive semiaxis length $a_{23} = 1.56$). The total interaction energy between building blocks is

$$U_{12} = 4\epsilon_0 \sum_{i=1}^{2} \sum_{j=1}^{2} \left[\epsilon_{\text{rep,i}}\epsilon_{\text{rep,j}} \left(\frac{\sigma_0}{r_{ij} - r_{ij}F_{1ij}^{-1/2} + \sigma_0} \right)^{12} - \right.$$
$$\left. -\epsilon_{\text{attr,i}}\epsilon_{\text{attr,j}} \left(\frac{\sigma_0}{r_{ij} - r_{ij}F_{2ij}^{-1/2} + \sigma_0} \right)^{6} \right], \quad (2)$$

where F_{1ij} and F_{2ij} are the 'repulsive' and 'attractive' elliptic contact functions [52], calculated between ellipsoids i and j, $\epsilon_{\text{rep}} = 1$ for both ellipsoids in the building block, and $\epsilon_{\text{attr,A}} = 0$, and $\epsilon_{\text{attr,B}} = 1$. The repulsive semiaxes for both ellipsoids are $a_{11} = a_{12} = a_{13} = 1.5$. The attractive semiaxes are not used for ellipsoid A (being purely repulsive in character), while for ellipsoid B they are $b_{21} = b_{22} = 1.5$, and $b_{23} = 1.56$. These semiaxes are employed for constructing the shape matrices, which define the repulsive and attractive

8

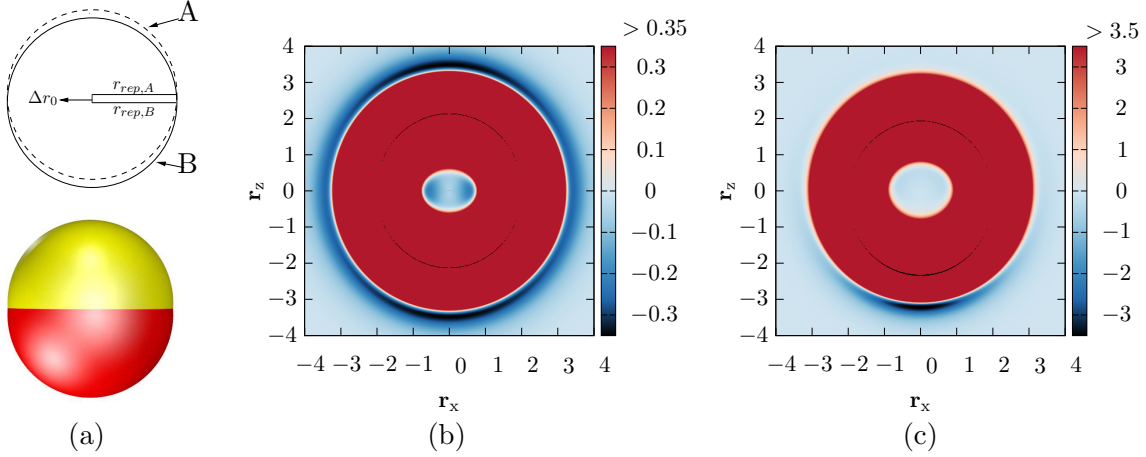elliptic contact functions.

B. Results

FIG. 3: (a) Schematic view and space-filling representation of the generic Janus-type building block. Dashed circle and yellow: ellipsoid A (purely repulsive), continuous circle and red: ellipsoid B (more attractive along its z axis). $\Delta r_0 = 0.2$, $r_{rep,A} = r_{rep,B} = 1.5$. (b) Potential energy surface of two parallel building blocks confined in the xz plane, with their principal axes aligned with the axes of that plane. (c) Same as (b), but with an antiparallel alignment of the z axes. Note that the energy range represented in (b) is ten times smaller than that in (c), and overlapping configurations with an interaction energy outside this range are coloured uniformly with the colour at the top of the range (red).

In this section we introduce a building block composed of two overlapping ellipsoids that strongly favours assembly into Bernal spirals (tetrahelices) [57, 58]. Our system behaves similarly to the experimental realisations of Janus particles [18] presented by Chen *et al.*, but the underlying energy landscape is likely rather different. In ref. [18] the authors demonstrate that the tetrahelix structures observed at high salt concentrations probably arise due to kinetic effects, and other tubular structures such as the 3(0,1,1) helix [58] are not observed because the basic unit of the tetrahelix (capped trigonal bipyramid, $N = 7$) forms first and it is sufficiently long-lived to aggregate into long chains. In contrast, our model ensures that tetrahelix structures are energetically favourable, and the interaction profile between building blocks makes the formation of alternative low-energy tubular packings impossible.

9

Hence we propose a new design, which we predict will guide assembly towards well-defined small helical structures very efficiently.

Figure 3a illustrates our Janus building block. Figures 3b and c provide a two-dimensional representation of the potential energy surfaces resulting from moving two building blocks in the xz plane, with their principal axes aligned, and with the z axes in parallel and antiparallel orientations, respectively. The potential is highly attractive at the pole of ellipsoid B furthest away from ellipsoid A. The interaction range is rather short, and the potential becomes isotropic and decays to zero rapidly as the distance between particles increases. The displacement by 0.1 distance units of the two ellipsoids is analogous to the experimental method of obtaining micrometre-sized Janus particles by coating silica spheres with gold [18, 59], since in that case the gold coating is thickest at the pole, and gradually decreases towards the equator. The hydrophobic interaction itself is determined by the monomolecular layer of alkanethiol applied on the gold coating, and is therefore constant on the surface of the patch. However, the net van der Waals interaction experienced by the particles is the strongest around the pole due to the greater thickness of the gold coating. The main difference between our model and the experimental setup is that the deviation from the spherical shape at the poles is about 1% for the experimental system, while in our case it is about 7%. Our potential is also softer than the usual hard sphere-square well representations for experimental colloidal Janus particles. Since we did not modify the original PY potential to incorporate Coulombic repulsion, our repulsive ellipsoid A has a short range, namely r^{-12}. We find that this repulsion is sufficient to disfavour close contacts between two repulsive ellipsoids, and gives rise to a force that tends to align two building blocks in an antiparallel fashion. The potential is continuous for every non-overlapping configuration. An additional benefit of using the same potential to describe both 'hemispheres' of the building blocks is that no explicit smoothing is required, which would otherwise be necessary to make the interaction profile and its derivative continuous around the hydrophobic-hydrophilic interface. There are discontinuities and unphysical minima in the potential corresponding to highly overlapping configurations, but moves that permit such overlaps are diagnosed and discarded in our global optimisation and pathway search algorithms. Overlaps between ellipsoidal particles are easily detected from the same elliptic contact function that arises in the energy evaluation. Such discontinuities and internal wells for overlapping configurations are common for anisotropic potentials [52, 60].
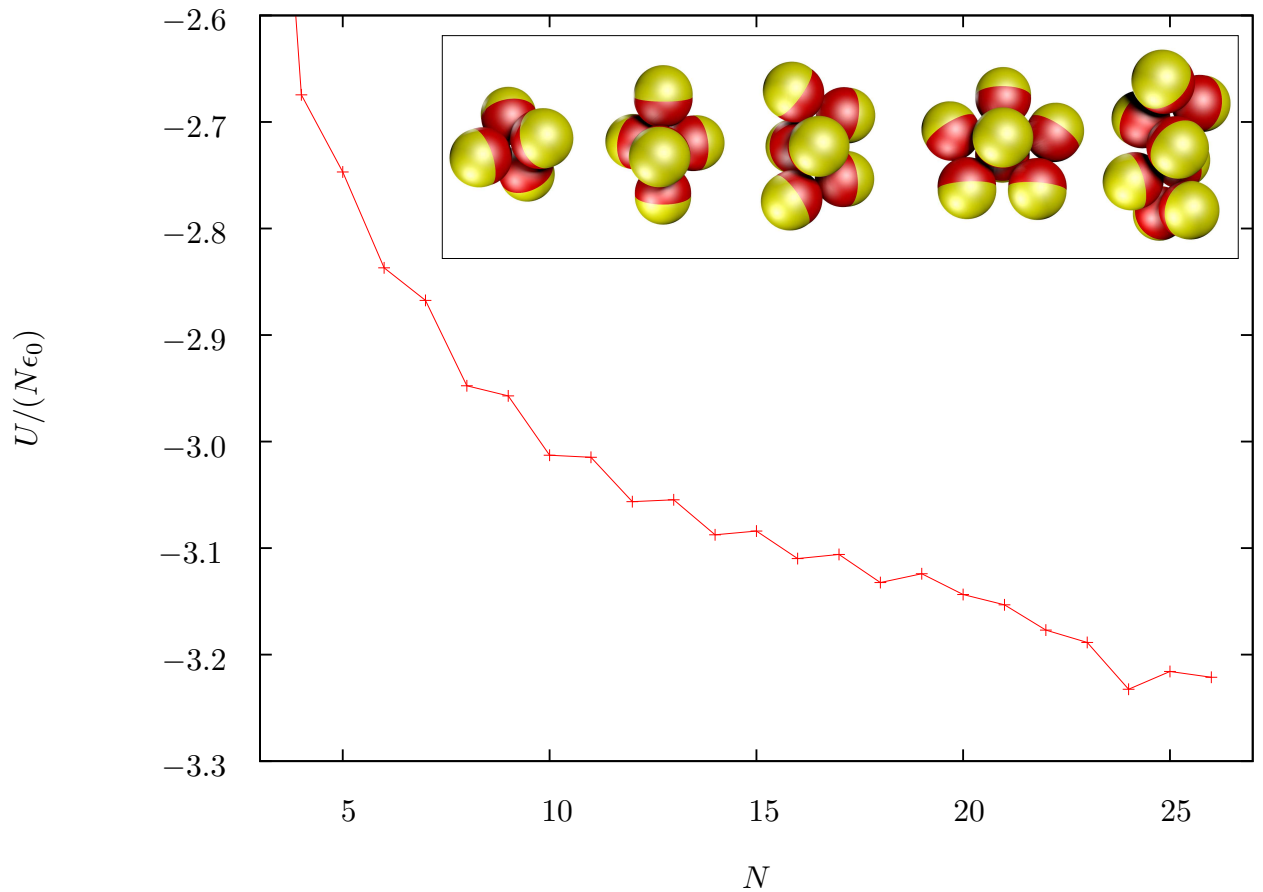
FIG. 4: Energy per particle for the predicted global minima in clusters containing between 4 and 26 Janus particles. The 'sawtooth' pattern showing a preference for even number clusters is due to the strongly bound dimer. Inset: lowest energy structures for small clusters ($N = 4$ to 8). 4: tetrahedral, 5: trigonal bipyramidal, 6: capped trigonal bipyramidal (CTBP), 7: pentagonal bipyramid, 8: Bernal spiral.

Our model Janus building blocks strongly prefer to interact *via* their attractive poles. Since the well depth is not uniform over the attractive half of the particle, dimerisation is favourable. An additional particle orients its attractive pole towards the dimer, but the short range and strong directionality of the interaction makes it impossible to form a strongly bound cluster. The most favourable geometry for the trimer therefore lacks a C_3 symmetry axis, and the geometry is slightly distorted (intercentre distances between the second ellipsoids of each building block are 3.02, 3.08 and 3.08, respectively). However, when the number of particles in the cluster is even, a complete set of dimers is possible. This pattern results in hierarchical assembly, where the dimers themselves behave as larger

11

building blocks, stacking along their attractive ellipsoids and rotated by 90 degrees. When highly symmetric clusters are possible, the strong dimer interactions can be disrupted if the extra stabilisation from the additional contacts can compete with the dimerisation energy. This situation arises for $N = 4$ and 5, with global minima corresponding to tetrahedral and trigonal bipyramidal structures, respectively. Increasing the cluster size further destabilises high symmetry configurations, and assemblies of dimers tend to be preferred. For example, the global minimum for $N = 6$ is a capped trigonal bipyramid (CTBP), not an octahedron, and starting from $N = 8$, the predicted global minima for every structure with an even number of particles are tetrahelices up to $N = 20$. We emphasise that these are not perfect tetrahelix structures, since the tetrahedral units are themselves somewhat distorted, the largest difference between the edges being around 7%. The strong preference for dimerisation gives rise to a characteristic 'sawtooth'-pattern in the energy per particle *versus* cluster size (Figure 4). The global minima for $N > 20$ are ring-like structures. There is recent experimental evidence for Janus particles preferring assembly into clusters with even numbers in two dimensions [61], and computational studies on a different Janus building block also show such a preference [62], giving rise to similar 'sawtooth' patterns.

Since there are essentially two types of interactions between the Janus building blocks in a tetrahelix, namely a stronger and a weaker attraction, assembly of such systems is intrinsically hierarchical through (i) dimerisation and (ii) association of dimers. Building blocks at either end of a finite strand are more weakly bound, so in a bulk system strand growth is preferred if there are free dimers available in solution. However, increasing the number of particles also allows for certain ring-like structures to arise, built up from tetrahedral units. For example, the predicted global minimum for 24 particles is 'doughnut'-shaped, corresponding to the first cyclic structure with high symmetry (D_{6d}). Interestingly, such structures have not yet been observed in experiment [18], although the main repeating unit in a tetrahelix is the CTBP structure [18], as in the cyclic global minimum predicted for 24 building blocks.

We have explored the energy landscape more extensively for clusters composed of 20 and 24 particles, using discrete path sampling [26–28] to grow databases of local minima and the transition states that connect them. The disconnectivity graphs constructed for the two cluster sizes are shown in Figures 5 and 8, respectively. We have used the same energy range, and positioned the tetrahelical minimum in the same part of the graph, so that the

12

two landscapes can be compared visually. Enantiomers are lumped together in these graphs.
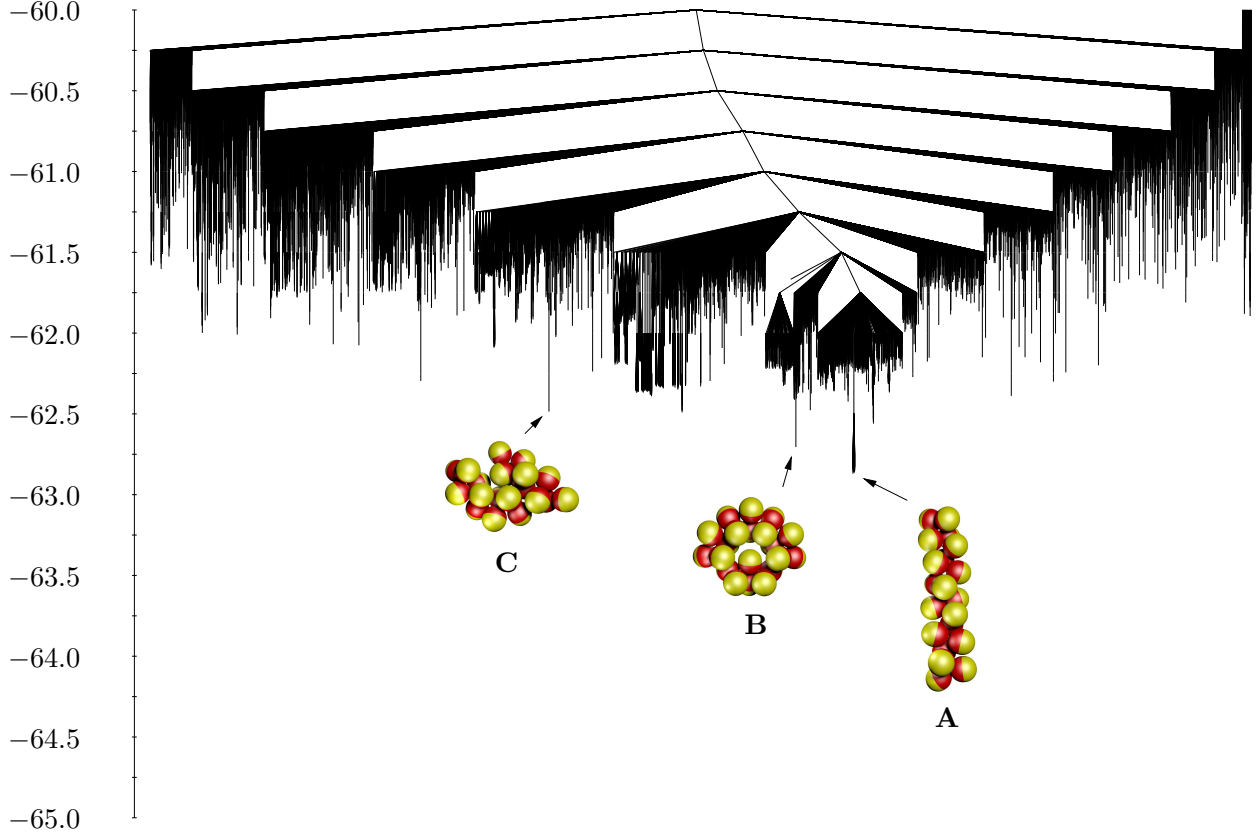

FIG. 5: Disconnectivity graph for $N = 20$ Janus building blocks. The global minimum is a Bernal spiral (**A**), which is very flexible. In this graph, more than 30 minima around the global minimum exhibit bent structures, which interconvert *via* 'hinge' motions. The lowest energy kinetic trap (**B**) corresponds to a symmetric cyclic structure, while the second-lowest (**C**) is a dimer of a low-energy minimum for $N = 10$.

For $N = 20$, we find that the tetrahelical global minimum is very flexible, with single transition state rearrangements resulting in bent structures that correspond to similar energies. The mechanism is a simple bending motion around a pair of particles strongly bound to each other in the helical structure, with the dimer acting as a hinge. Only strongly bound dimers act as hinges, with their attractive poles almost antiparallel. Kinetically this is a favourable rearrangement, with relatively low barriers below $0.25\,\epsilon_0$. Such 'hinge'-rearrangements are characteristic low-energy transitions between worm-like structures, and are preferred due to the fact that the binding pattern of dimers does not change, i.e. no dimeric binding configuration is disturbed. The identified 'hinge'-rearrangements resemble those found for sodium

chloride clusters [63], where such rearrangements have relatively high barriers.

'Hinge' rearrangement mechanisms are preferred during chirality inversion as well. Figure 6 and Supplementary Movie 2 illustrate one of the fastest pathways between a left-handed and a right-handed $N = 24$ helix. All such pathways involve exclusively 'hinge'-motions and a minimum of five transition states. Such sequential rearrangements have been observed experimentally for smaller clusters [18], and we see exactly the same type of cooperative pathways, resulting in propagation of the change in handedness along the chain.
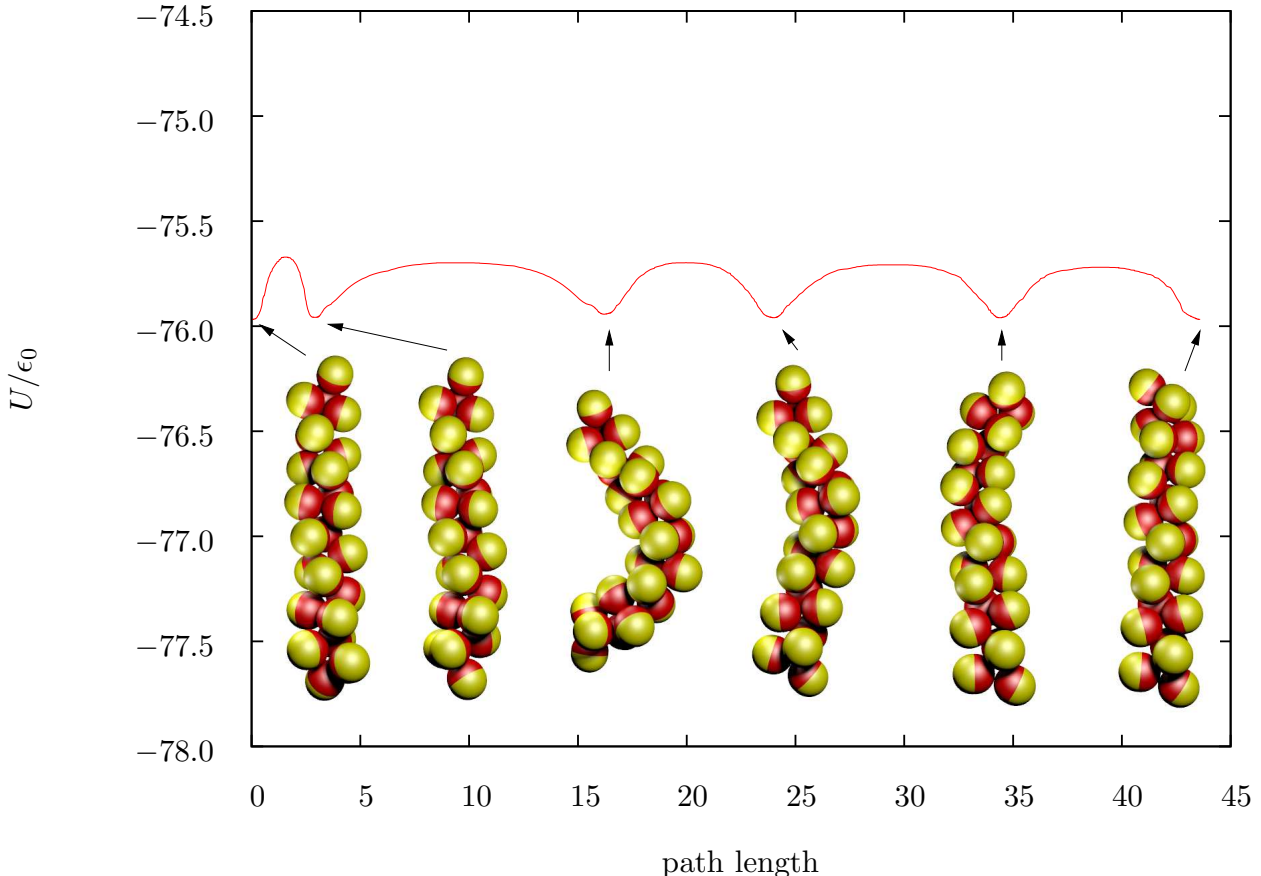

FIG. 6: Predicted fastest pathway for inversion of a 24-particle tetrahelix structure, consisting exclusively of 'hinge' rearrangements. The fourth minimum in the path is in fact a dimer composed of a left-handed and a right-handed $N = 12$ helix.

The disconnectivity graph for $N = 20$ contains many kinetic traps, the lowest of which is a ring structure with a symmetry plane (**B**). Other low-energy minima that appear as traps are again aggregates of dimers, and contain two or more CTBP units. The structure **C** depicted in Figure 5 is in fact a dimer of the second-lowest potential energy minimum
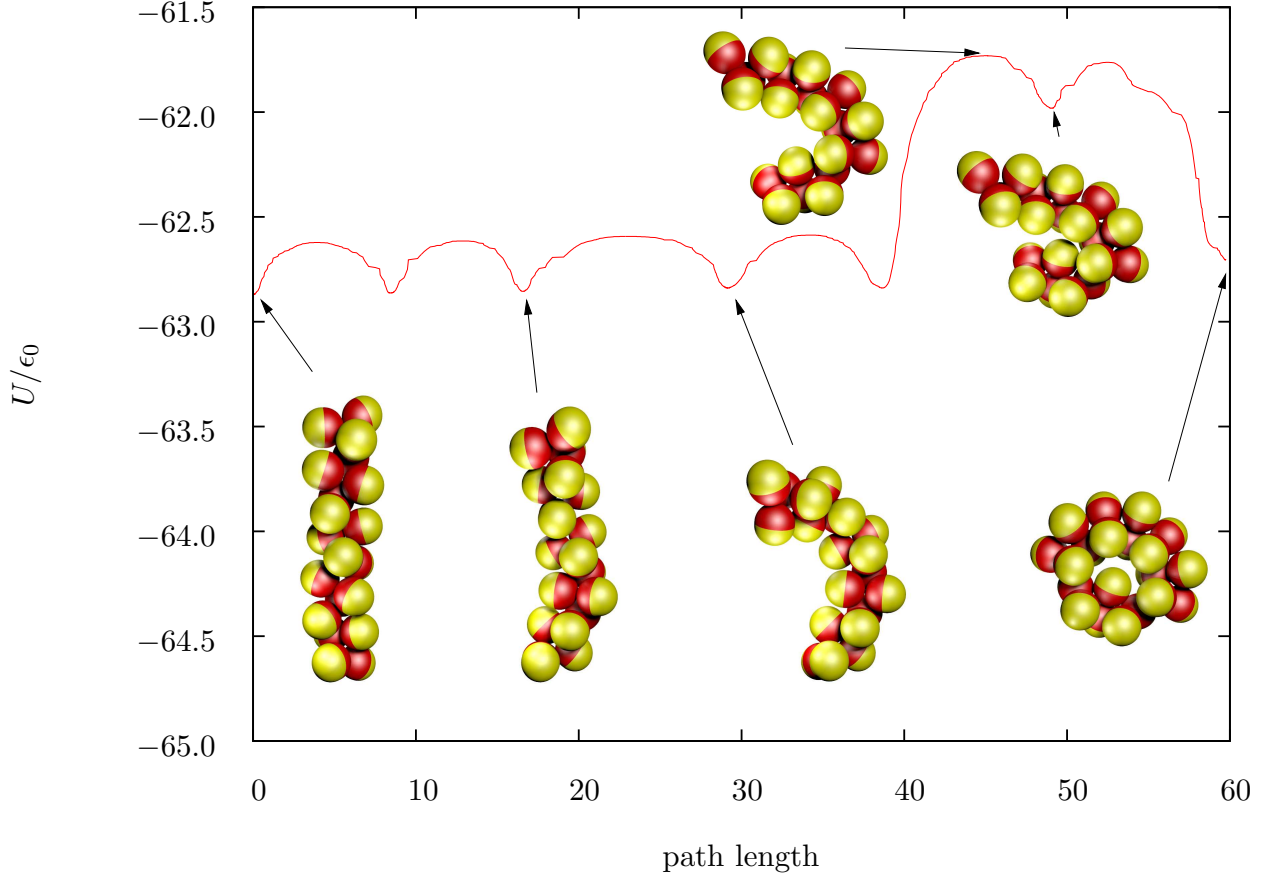
14

predicted for the $N = 10$ cluster.

FIG. 7: Fastest pathway between the tetrahelix global minimum and a low-energy closed ring structure. The rearrangements with energy barriers of about $0.25\,\epsilon_0$ are all 'hinge'-motions. Structures for selected minima and the highest energy transition state are also shown.

The fastest pathway between the helical global minimum and the ring structure predicted to act as a kinetic trap also proceeds through low-energy 'hinge' mechanisms (Figure 7, see also Supplementary Movie 1) up to a point, and the high energy of the fifth transition state and the fifth minimum along the pathway is due to the torsional strain introduced when the attractive interactions between two adjacent dimer units are lost (rotation of a dimer around the intercentre vector defined by two loosely bound neighbour particles). The final rearrangement in the overall pathway is again a 'hinge' mechanism.

Helical structures are much higher in energy for $N = 24$ clusters than the 'doughnut'-shaped global minimum. Although they exhibit the same flexibility as for $N = 20$, the energetic separation from the rest of the landscape is not as pronounced, and these structures
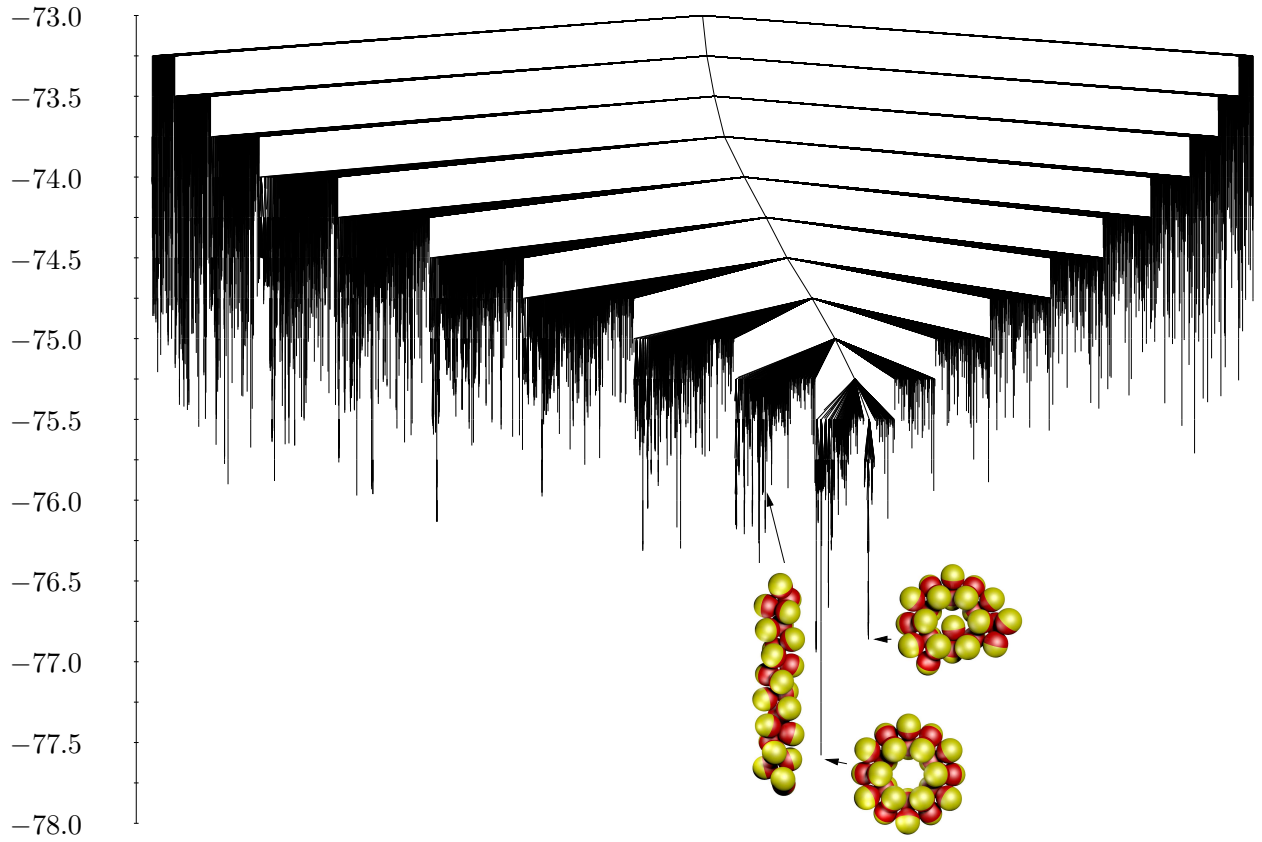
FIG. 8: Disconnectivity graph for $N = 24$ Janus building blocks. The global minimum is a ring structure with D_{6d} symmetry.

can easily undergo ring closures. However, the highly symmetric global minimum cannot be reached through simple low-energy 'hinge' rearrangements. At least one step involving a change in dimerisation pattern has to occur at one end of the helix, during which the particles in two adjacent dimers rotate cooperatively to change the strong bonding into a weak interaction and *vice versa*. Such particle rotations result in an energy barrier of about $1\,\epsilon_0$ at the end of the chain, which would be much higher if they occurred within the chain. The fastest overall pathway between the helical structure and the global minimum is shown in Figure 9 and Supplementary Movie 3.

It would be interesting to investigate how the helical clusters of Janus building blocks designed in ref. [18] behave in dilute solutions, where chain growth is less likely. Although chirality inversion has been observed for such helices, all other reported transformations involve chain growth. The 'hinge' mechanisms observed experimentally hint at other possible rearrangements for longer helices. In our model system, the lowest energy transformations
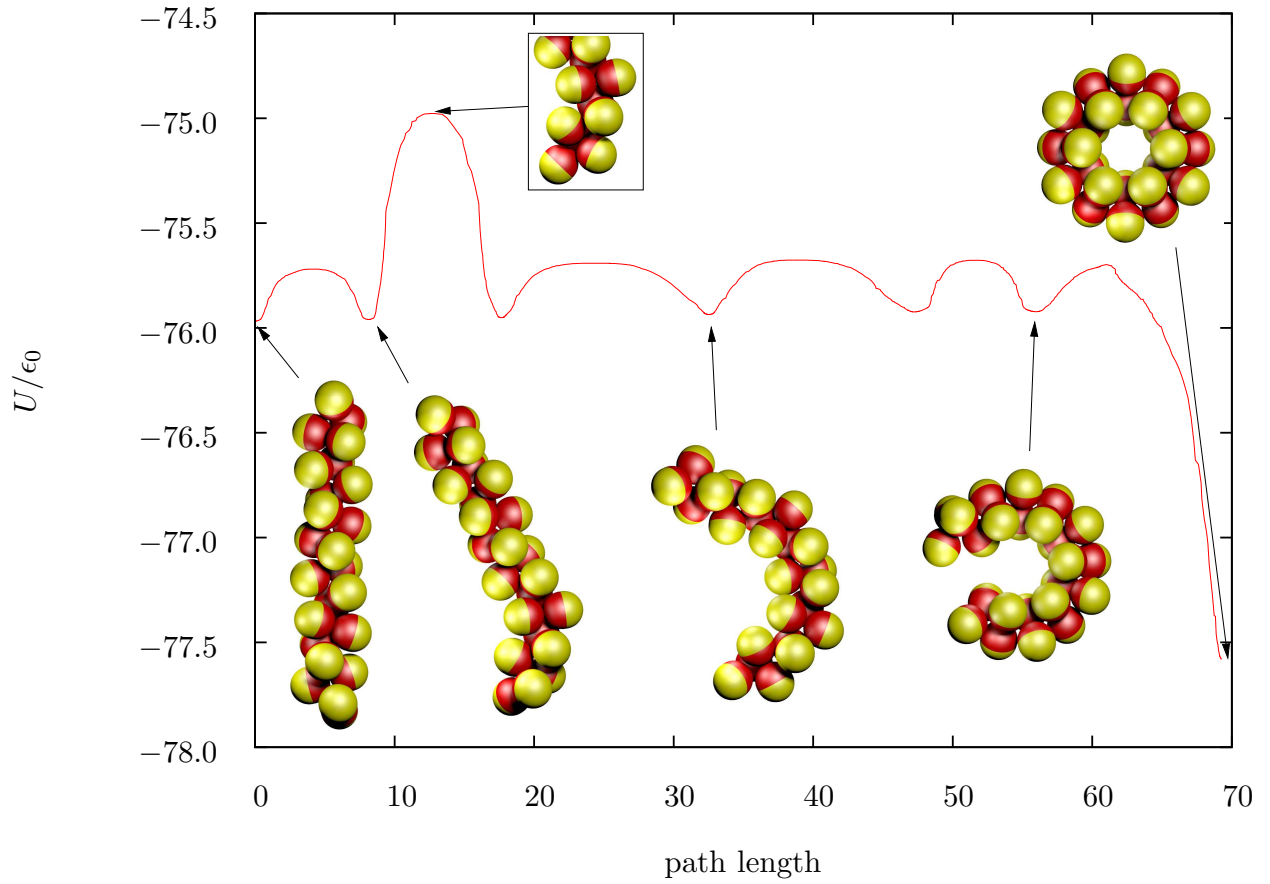
16

FIG. 9: Fastest pathway between the 'doughnut'-shaped global minimum of D_{6d} symmetry and the tetrahelix structure. The rearrangements involved with energy barriers of about $0.25\,\epsilon_0$ all correspond to 'hinge' mechanisms. Structures are shown for selected minima. The inset shows a part of the cluster in the high energy transition state involving change in the dimerisation pattern.

involve only 'hinge' motions. By increasing the temperature, barriers could be overcome for the less favoured rearrangements (similar to those described above), and in dilute solutions highly symmetric rings might form.

It remains to be seen how our model building blocks behave in a bulk phase. Based on the global optimisation data and on the energy landscape analysis for $N = 20$ and 24, a kinetically controlled seeded growth of helices is likely above 20 particles, by sequential addition of dimers or CTBP units. Assembly of short helices containing even numbers of particles will be thermodynamically preferred.

17

V. CONCLUSIONS

We have presented two contrasting theoretical designs for self-assembling helical nanostructures. First we described the assembly of charged asymmetric dipolar dumbbells into a helix subject to an external magnetic field. Here, helix formation is due to the competition between screened electrostatic repulsion and magnetic dipolar interactions. We demonstrate that significant control over the helical pitch length (around 30%) can be achieved by tuning the balance between these two interactions. This tuning is achieved by varying the range of the screened electrostatic interactions, which can be realised experimentally by modulating the salt concentration of the medium.

We then analysed a model Janus building block that dimerises, where the dimers self-assemble into Bernal spirals, simply by allowing for a strong short-range interaction close to the attractive pole of the particle. Large-scale rearrangement mechanisms of such spirals involve sequential 'hinge' motions.

In agreement with previous work, we find that the formation of complex mesoscopic structures is primarily driven by the anisotropy of building block shape and interactions [51, 53]. Our model of rigidly linked ellipsoids can capture a wide range of anisotropy, and the self-assembling behaviour for certain sizes is a direct consequence of the building block properties. The model can easily be parameterised to allow for larger overlap between building blocks, in order to model 'softer' Janus particles.

The two models presented here provide two very different approaches to achieve self-assembly into helical structures from anisotropic building blocks on the colloidal length scale. In both models, helicity is the direct consequence of the shape and interaction anisotropies of the building blocks. The overall interaction strength between two particles depends on their relative orientation, and on the balance between the repulsive and attractive forces, which can be tuned experimentally, for example by varying the ionic strength of the solution. The dumbbell model illustrates that varying such experimental conditions makes it possible to directly control the helical pitch, while the Janus model provides an example of a building-block design that facilitates hierarchical self-assembly into helical structures. Both models and approaches are relatively simple, and we therefore believe that they are should be realisable experimentally.

VI. ACKNOWLEDGEMENTS

---

[1] V. Percec, M. Glodde, T. K. Bera, Y. Miura, I. S. I, K. D. Singer, V. S. Balagurusamy, P. A. Heiney, I. Schnell, A. R. A, et al., Nature **419**, 384 (2002).

[2] E. Yashima, K. Maeda, H. Iida, Y. Furusho, and K. Nagai, Chem. Rev. **109**, 6102 (2009).

[3] D. Pijper and B. L. Feringa, Soft Matter **4**, 1349 (2008).

[4] T. E. Gier, X. Bu, P. Feng, and G. D. Stucky, Nature **395**, 154 (1998).

[5] J.-M. Lehn, Science **295**, 2400 (2002).

[6] S. C. Glotzer and M. J. Solomon, Nature Mater. **6**, 557 (2007).

[7] S. Sacanna, W. T. M. Irvine, P. M. Chaikin, and D. J. Pine, Nature **464**, 575 (2010).

[8] Y. Min, M. Akbulut, K. Kristiansen, Y. Golan, and J. Israelachvili, Nature Mater. **7**, 527 (2008).

[9] D. Chakrabarti, S. N. Fejer, and D. J. Wales, Proc. Natl. Acad. Sci. USA **106**, 20164 (2009).

[10] D. Zerrouki, J. Boudri, D. Pine, P. Chaikin, and J. Bibette, Nature **455**, 380 (2008).

[11] J. D. Watson and F. H. C. Crick, Nature **171**, 737 (1953).

[12] S. E. Howson, A. Bolhuis, V. Brabec, G. J. Clarkson, J. Malina, A. Rodger, and P. Scott, Nature Chem. **4**, 31 (2012).

[13] S. Srivastava, A. Santos, K. Critchley, K.-S. Kim, P. Podsiadlo, K. Sun, J. Lee, C. Xu, D. Lilly, S. C. Glotzer, et al., Science **327**, 1355 (2010).

[14] L. Hong, A. Cacciuto, E. Luijten, and S. Granick, Langmuir **24**, 621 (2008).

[15] Z.-W. Li, Z.-Y. Lu, Z.-Y. Sun, and L.-J. An, Soft Matter **8**, 6693 (2012).

[16] Y. Liu, W. Li, T. Perez, J. D. Gunton, and G. Brett, Langmuir **28**, 3 (2012).

[17] W. Li and J. D. Gunton, Langmuir **29**, 8517 (2013).

[18] Q. Chen, J. K. Whitmer, S. Jiang, S. C. Bae, E. Luijten, and S. Granick, Science **331**, 199 (2011).

[19] A. I. Campbell, V. J. Anderson, J. S. van Duijneveldt, and P. Bartlett, Phys. Rev. Lett. **94**, 208301 (2005).

[20] S. Mossa, F. Sciortino, P. Tartaglia, and E. Zaccarelli, Langmuir **20**, 10756 (2004).

[21] F. Sciortino, P. Tartaglia, and E. Zaccarelli, J. Phys. Chem. B **109**, 21942 (2005).

[22] Z. Li and H. A. Scheraga, Proc. Natl. Acad. Sci USA. **84**, 6611 (1987).

[23] D. J. Wales and J. P. K. Doye, J. Phys. Chem. A **101**, 5111 (1997).

[24] D. J. Wales and H. A. Scheraga, Science **285**, 1368 (1999).

[25] D. J. Wales, *GMIN: A program for finding global minima and calculating thermodynamic properties from basin-sampling,*, http://www-wales.ch.cam.ac.uk/GMIN (????).

[26] D. J. Wales, Mol. Phys. **100**, 3285 (2002).

[27] D. J. Wales, Mol. Phys. **102**, 891 (2004).

[28] D. J. Wales, Int. Rev. Phys. Chem. **25**, 237 (2006).

[29] D. J. Wales, *OPTIM: A program for characterising stationary points and reaction pathways*, http://www-wales.ch.cam.ac.uk/OPTIM, http://www-wales.ch.cam.ac.uk/OPTIM (2005).

[30] D. J. Wales, *PATHSAMPLE: A program for refining and analysing kinetic transition networks*, http://www-wales.ch.cam.ac.uk/PATHSAMPLE (2005).

[31] S. A. Trygubenko and D. J. Wales, J. Chem. Phys. **120**, 2082 (2004).

[32] G. Henkelman and H. Jónsson, J. Chem. Phys. **111**, 7010 (1999).

[33] G. Henkelman, B. P. Uberuaga, and H. Jónsson, J. Chem. Phys. **113**, 9901 (2000).

[34] G. Henkelman and H. Jónsson, J. Chem. Phys. **113**, 9978 (2000).

[35] S. A. Trygubenko and D. J. Wales, J. Chem. Phys. **120**, 2082 (2004).

[36] L. J. Munro and D. J. Wales, Phys. Rev. B **59**, 3969 (1999).

[37] E. Dijkstra, Numer. Math. **1**, 269 (1959).

[38] O. M. Becker and M. Karplus, J. Chem. Phys. **106**, 1495 (1997).

[39] D. J. Wales, M. A. Miller, and T. R. Walsh, Nature **394**, 758 (1998).

[40] D. J. Wales, *Energy Landscapes: Applications to Clusters, Biomolecules and Glasses* (Cambridge University Press, 2003).

[41] D. J. Wales, Curr. Op. Struct. Biol. **20**, 3 (2010).

[42] D. J. Wales, Phil. Trans. Roy. Soc. A **370**, 2877 (2012).

[43] M. O. Robbins, K. Kremer, and G. S. Grest, J. Chem. Phys. **88**, 3286 (1988).

[44] H. Löwen and G. Kramposthuber, Europhys. Lett. **23**, 673 (1993).

[45] A. Yethiraj and A. van Blaaderen, Nature **421**, 513 (2003).

[46] H. Löwen, A. Esztermann, A. Wysocki, E. Allahyarov, R. Messina, A. Jusufi, N. Hoffmann, D. Gottwald, G. Kahl, M. Konieczny, et al., J. Phys.: Conf. Series **11**, 207 (2005).

[47] A. van Blaaderen, M. Dijkstra, R. van Roij, A. Imhof, M. Kamp, B. W. Kwaadgras, T. Vissers, and B. Liu, Eur. Phys. J. Special Topics **222**, 2895 (2013).

[48] S. K. Smoukov, S. Gangwal, M. Marquezbc, and O. D. Velev, Soft Matter **5**, 1285 (2009).

[49] A. Ivlev, H. Löwen, G. Morfill, and C. P. Royall, *Complex Plasmas and Colloidal Dispersions: Particle-Resolved Studies of Classical Liquids and Solids* (World Scientific, London, 2012).

[50] J. N. Israelachvili, *Intermolecular and Surface Forces* (Academic Press, London, 2011).

[51] S. N. Fejer, D. Chakrabarti, and D. J. Wales, Soft Matter **7**, 3553 (2011).

[52] L. Paramonov and S. N. Yaliraki, J. Chem. Phys. **123**, 194111 (2005).

[53] S. N. Fejer, D. Chakrabarti, and D. J. Wales, ACS Nano **4**, 219 (2010).

[54] S. W. Olesen, S. N. Fejer, D. Chakrabarti, and D. J. Wales, RSC Adv. **3**, 3553 (2011).

[55] D. J. Wales, Phil. Trans. Roy. Soc. A **363**, 357 (2005).

[56] D. Chakrabarti and D. J. Wales, Phys. Chem. Chem. Phys. **11**, 1970 (2009).

[57] A. H. Boerdijk, Philips Res. Rep. **7**, 303 (1952).

[58] R. O. Erickson, Science **181**, 705 (1973).

[59] Q. Chen, E. Diesel, J. K. Whitmer, S. C. Bae, E. Luijten, and S. Granick, Journal of the American Chemical Society **133**, 7725 (2011).

[60] J. G. Gay and B. J. Berne, J. Chem. Phys. **74**, 3306 (1981).

[61] Y. Iwashita and Y. Kimura, Soft Matter **9**, 10694 (2013).

[62] Z. Preisler, T. Vissers, F. Smallenburg, G. Muna, and F. Sciortino, J. Phys. Chem. B **117**, 9540 (2013).

[63] J. P. K. Doye and D. J. Wales, Phys. Rev. B **59**, 2292 (1999).